

# EndoOmni: Zero-Shot Cross-Dataset Depth Estimation in Endoscopy by Robust Self-Learning from Noisy Labels

Qingyao Tian, Zhen Chen, Huai Liao, Xinyan Huang, Lujie Li, Sébastien Ourselin, Hongbin Liu

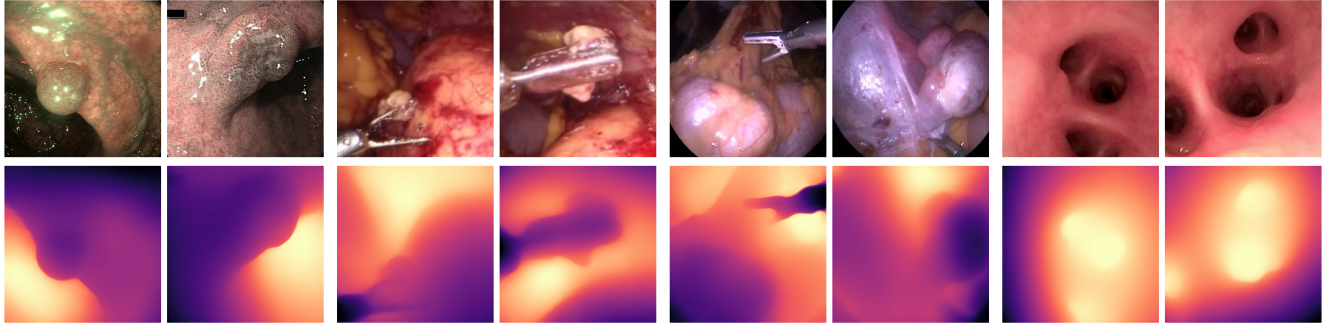


Fig. 1: EndoOmni demonstrates exceptional zero-shot performance across various unseen endoscopy datasets: **(a)** the OBR dataset [1], **(b)** the da Vinci surgical dataset [2], **(c)** the Heico dataset [3], and **(d)** our own bronchoscopy data collected from porcine models. The scenes encompass a range of environments, including tubular structures, complex surgical tools and intricate lumen hierarchy.

**Abstract**—Single-image depth estimation is essential for endoscopy tasks such as localization, reconstruction, and augmented reality. Most existing methods in surgical scenes focus on in-domain depth estimation, limiting their real-world applicability. This constraint stems from the scarcity and inferior labeling quality of medical data for training. In this work, we present EndoOmni, the first foundation model for zero-shot cross-domain depth estimation for endoscopy. To harness the potential of diverse training data, we refine the advanced self-learning paradigm that employs a teacher model to generate pseudo-labels, guiding a student model trained on large-scale labeled and unlabeled data. To address training disturbance caused by inherent noise in depth labels, we propose a robust training framework that leverages both depth labels and estimated confidence from the teacher model to jointly guide the student model training. Moreover, we propose a weighted scale-and-shift invariant loss to adaptively adjust learning weights based on label confidence, thus imposing learning bias towards cleaner label pixels while reducing the influence of highly noisy pixels. Experiments on zero-shot relative depth estimation show that our EndoOmni improves state-of-the-art methods in medical imaging for 41% and existing foundation models for 25% in terms of absolute relative error on specific dataset. Furthermore, our model provides strong initialization for fine-tuning to metric depth estimation, maintaining superior

Qingyao Tian is with Institute of Automation, Chinese Academy of Sciences, Beijing, China, and also with the School of Artificial Intelligence, University of Chinese Academy of Sciences, Beijing, China.

Zhen Chen is with Centre of AI and Robotics, Hong Kong Institute of Science & Innovation, Chinese Academy of Sciences, HK, China.

Huai Liao, Xin-yan Huang and Lujie Li are with The First Affiliated Hospital of Sun Yat-sen University, Guangzhou, Guangdong, China.

Sébastien Ourselin is with the School of Engineering and Imaging Sciences, King’s College London, UK.

Corresponding author: Hongbin Liu is with Institute of Automation, Chinese Academy of Sciences, and with Centre of AI and Robotics, Hong Kong Institute of Science & Innovation, Chinese Academy of Sciences. He is also affiliated with the School of Engineering and Imaging Sciences, King’s College London, UK. (e-mail: liuhongbin@ia.ac.cn).

This work has been submitted to the IEEE for possible publication. Copyright may be transferred without notice, after which this version may no longer be accessible.

performance in both in-domain and out-of-domain scenarios. The source code will be publicly available.

**Index Terms**—Endoscopy, monocular depth estimation, foundation models, zero-shot generalization

## I. INTRODUCTION

Depth estimation is a critical task for numerous applications such as 3D reconstruction, localization and augmented reality visualization [4]–[6]. In the realm of single-image depth estimation (SDE) for natural images, significant strides have been made toward developing generalizable foundation models across various datasets [7]–[10]. Their efficacy stems from extensive training on large-scale datasets, enabling versatile representation learning.

However, the SDE in endoscopic imagery remains largely domain-specific, suffering from poor generalization and limited real-world application. Despite some efforts to adapt foundation models trained on natural imagery for medical depth estimation, these are limited in scope and primarily experimental [11]–[13]. The disparity in research focus between natural and medical imaging can be attributed to two challenges inherent in medical datasets: **1) data scarcity** and **2) inferior labeling quality** [14]. These factors result in models that are prone to overfitting and struggle to generalize to unseen data [15].

This study aims to develop a foundation model for endoscopic SDE by addressing these challenges, enabling robust zero-shot performance across diverse datasets while offering fine-tuning for state-of-the-art metric depth estimation.

Addressing the limitation of data scarcity, we have assembled the most extensive meta-dataset for medical image SDE, encompassing over 200,000 labeled frames from public and proprietary datasets and an additional 500,000

unlabeled frames (Table I) for model training and evaluation. To harness the potential of unlabeled data, we leverage an self-learning strategy that utilizes a pretrained teacher model to generate pseudo labels. This combined labeled and pseudo-labeled data is then used to train a student model that processes highly perturbed images. This self-learning framework enhances training data variety, promoting generalization by exposing the model to diverse features and patterns. However, since the teacher model predicts for out-of-domain datasets, the resulting pseudo labels are often noisy, posing an additional challenge for robust training.

To handle noisy labels, previous SDE studies have introduced a trimming strategy for loss calculation, where outliers are detected and removed by trimming the largest residuals in each instance [7]. While this strategy contributes to training stability, it tends to neglect challenging image regions. The recent Depth Anything v2 [10] also recognized the performance drop due to label noise and suggested using synthetic data and a stronger pretrained teacher model for training. However, these solutions are impractical in the medical imaging domain due to the lack of large synthetic datasets and the unavailability of strong pretrained models.

In this work, we pursue a refined self-learning framework and a robust training loss to guide network training by noisy labels and pseudo labels. We creatively extend the line of thinking in robust training on classification problems [16]–[18] to the challenge of depth estimation. Through our empirical experiments, we observe that loss on clean data converges faster due to the inherent consistency of clean labels. Additionally, pseudo-labels tend to be more reliable when the teacher model predicts consistent results for the same instance across different augmentations. Based on this analysis, we propose estimating per-pixel label confidence according to the teacher model’s learning behavior, and using both labels and confidence to jointly guide the training of student model. Moreover, we have developed a robust SDE training loss that adjusts learning weights based on estimated label confidence. This approach not only mitigates training instability caused by label noise but also maintains the contribution of difficult regions in each instance, thereby enhancing the learning effectiveness of the SDE network.

In summary, the contributions of this work are as follows:

- We present EndoOmni, the first foundation model for zero-shot cross-dataset depth estimation of endoscopic imagery, by leveraging the potential of large-scale comprehensive endoscopy data.
- We propose a robust self-learning framework where a student model learns from a mix of labeled and unlabeled data, guided by the label confidence derived from analyzing the teacher model’s learning behavior.
- We address the disturbance of noisy labels by proposing a weighted scale-and-shift-invariant training loss. This approach adjusts learning weights based on estimated label confidence, promoting learning bias towards clean labels and ensuring robust training.
- Our model exceeds existing methods in medical imaging and foundation models in zero-shot relative depth esti-

TABLE I: Mixing dataset overview.

Dataset	Organs	Size
Labeled		
Hamlyn Centre Datasets <sup>†</sup>	Kidney	91,866 fr.
C3VD [19]	Colon phantom	8,742 fr.
SERV-CT [20]	Liver, kidney, heart	32 fr.
EndoAbS [21]	Liver, kidney, spleen	120 fr.
SCARED [22]	Abdomen	22,950 fr.
SimColon [23]	Colon simulation	16,016 fr.
Ours-Phantom	Airway phantom	395 fr.
Ours-Patient	Airway	70,223 fr.
Unlabeled		
EndoSLAM [24]	Colon, stomach, etc.	42,459 fr.
EndoMapper [25]	Colon	241,887 fr.
ROBUST-MIS [26]	Abdomen	128,501 fr.
EAD [27]	Stomach, ureter, etc.	2,531 fr.
Surgical-Vis [28]	-	3,360 fr.
CholecT50 [25]	Abdomen	100,863 fr.
CVC-ClinicDB [29]	Colon	612 fr.

Dataset size refers to the number of image frames actually used. Original datasets might be selectively extracted to ensure variability.

mation with a large margin. Furthermore, it maintains superior performance in both in-domain and out-of-domain scenarios fine-tuned to metric depth estimation.

## II. RELATED WORKS

Our main contribution is a foundation model for single-image depth estimation (SDE) in endoscopy by learning from noisy labels. Thereby, we review related works on cross dataset SDE, SDE in endoscopy and robust learning.

**Cross Dataset SDE.** Contrary to works that learn depth estimation model for a single dataset [30]–[32], emerging research [7]–[9], [33] has explored training SDE models or pretraining flagship models on mixing dataset. The pioneering work by MiDaS [7] introduced affine-invariant loss, allowing for scale-and-drift agnostic depth learning across datasets, thus mitigating the variance in depth distributions. Subsequent developments, such as DPT [8], have leveraged more complex architectures like the vision transformer to further enhance model performance. Depth Anything [9] extended this paradigm by incorporating unlabeled data into the training process, which significantly boosted the performance of MDE models. While these models initially predict only relative depth, their ability to adapt to metric depth estimation through fine-tuning has demonstrated superior performance compared to models trained on isolated datasets.

**SDE in Medical Endoscopy.** SDE in endoscopic images aids in precise navigation, accurate lesion assessment, and improved surgical planning. Given the impracticality of using depth cameras or LiDAR in such settings, most datasets depend on correlating endoscopic views with pre-operative CT scans or generating sparse point clouds via calibrated stereo-endoscopes. However, the limited availability of training data remains a significant barrier. As a result, existing research of SDE in medical imaging put extra effort into learning through view synthesis [24], [34]–[36] and generative models

<sup>†</sup> <http://hamlyn.doc.ic.ac.uk/vision/>

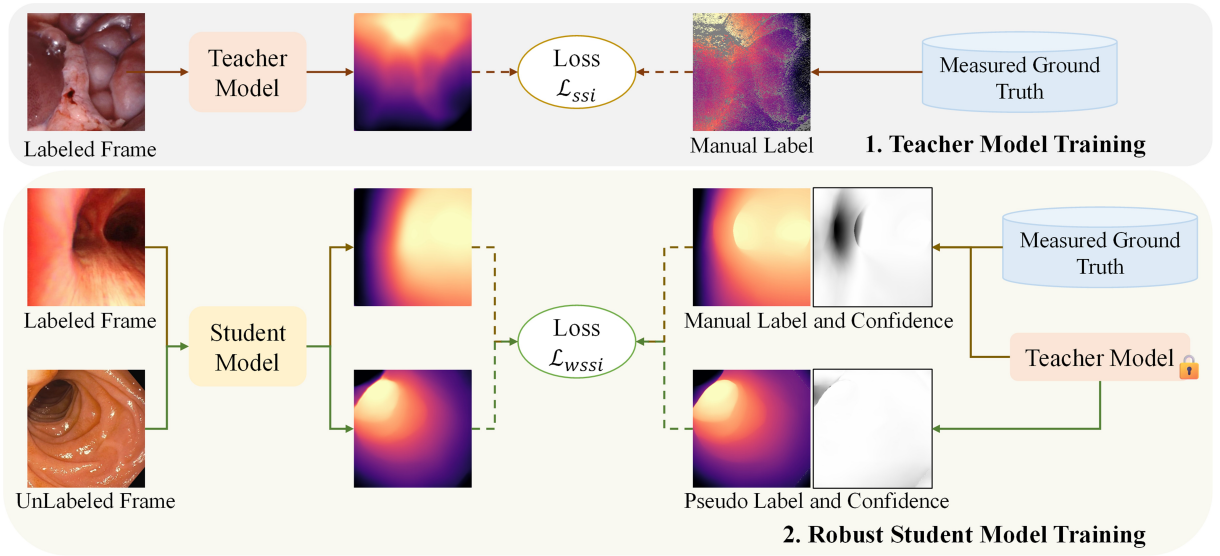


Fig. 2: Training framework of EndoOmni: A teacher network is first trained on labeled datasets. Sequentially, a student model is trained on a mix of labeled and unlabeled data, leveraging our robust learning loss guided by the pretrained teacher model. This diverse data and robust training framework enhances the student model’s generalization ability.

[37]–[40] to estimate depth for individual datasets or to enhance unsupervised training efficacy. With the success of foundation models and their outstanding performance in zero-shot SDE, a few recent works attempted to adapt foundation models trained on natural images to medical imaging [11], [12]. However, due to the large domain gap between medical images and natural images, zero-shot generalization of these foundation models are not as good as expected [13].

**Learning with Noisy Labels.** Noisy labels are a frequent issue in real-world datasets, particularly in medical imaging, where accurate annotations are costly and not always accessible. Despite the substantial performance gains deep neural networks achieve with large volumes of training data, their training processes remain susceptible to overfitting when exposed to noisy labels [41]. Learning robustly through noisy annotations is thus an important topic. Prior works on robust network learning primarily focus on classification tasks [16]–[18]. Fewer SDE studies have focused on dealing with false annotations. Notably, [7] introduced a trimming strategy for loss calculation. In this approach, outliers are detected and removed by trimming the largest loss residuals in each instance. While this method is effective in many cases, it also removes loss components where the network’s estimation significantly deviates from the ground truth, making harder-to-learn cases even more challenging.

In this study, we have curated the largest meta-dataset for endoscopy SDE and trained our EndoOmni model on this extensive mixed dataset. To mitigate label noise, we introduce a self-learning framework that uses both (pseudo) labels and their associated confidence map to guide network training. Additionally, we propose a weighted scale-and-shift-invariant loss to concentrate gradient updates on regions with high confidence labels.

### III. METHODOLOGY

In this study, we establish a robust training framework that utilizes both labeled and unlabeled data for SDE network training. The process starts by training a teacher model  $g$  on labeled datasets. Subsequently, a student model  $f$  is trained using a combination of labeled data  $X^l = \{(\mathbf{x}_n^l, \mathbf{z}_n)\}_{n=1}^N$  and unlabeled data  $X^u = \{\mathbf{x}_m^u\}_{m=1}^M$ . The teacher model  $g$  supports this process by generating pseudo-labels for the unlabeled data and assessing label confidence for both manually annotated and pseudo labels. The training framework of EndoOmni is illustrated in Fig. 2.

#### A. Teacher Model Training

Following [7]–[9], we convert depth labels into disparity space  $\mathbf{d} = \frac{1}{z}$  and normalize these within the range 0 to 1 for each depth map. To facilitate training across various datasets without the interference of inconsistent scale and shift factors across datasets, we train the teacher model with scale-and-shift invariant (SSI) loss [7]:

$$L_{ssi} = \frac{1}{HW} \sum_{i=1}^{HW} \rho(\hat{\mathbf{d}}_i, \mathbf{d}_i), \quad (1)$$

where  $\hat{\mathbf{d}} = g(x)$  and  $\mathbf{d}$  represent the predicted and ground truth depth, respectively.  $H$  and  $W$  are the image height and width.  $\rho$  is formulated as:

$$\rho(\hat{\mathbf{d}}, \mathbf{d}) = |\hat{\mathbf{d}}^* - \mathbf{d}^*|. \quad (2)$$

Here,  $\hat{\mathbf{d}}^*$  and  $\mathbf{d}^*$  are calculated by aligning the prediction  $\hat{\mathbf{d}}$  and ground truth  $\mathbf{d}$  to have zero translation and unit scale:

$$\mathbf{d}^* = \frac{\mathbf{d} - t(\mathbf{d})}{s(\mathbf{d})}, \quad \hat{\mathbf{d}}^* = \frac{\hat{\mathbf{d}} - t(\hat{\mathbf{d}})}{s(\hat{\mathbf{d}})}, \quad (3)$$

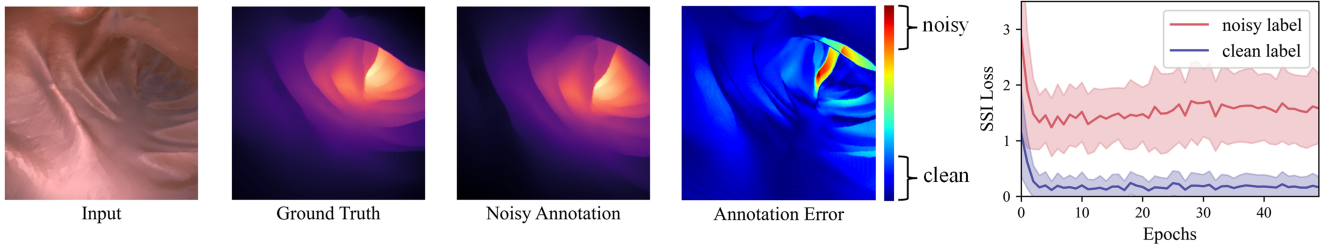


Fig. 3: Model learning dynamics. Noisy annotations are created by misaligning image frames with ground truth depth labels. Annotation error is the L1 distance between ground truth and noisy annotations. Clean and noisy pixels are sampled based on annotation error, with loss convergence shown as mean  $\pm$  standard deviation. The loss on clean pixels quickly converges, while it remains higher on noisy pixels throughout training.

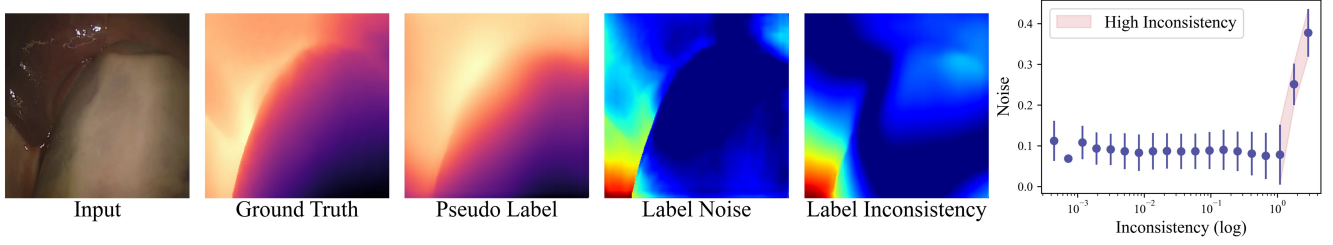


Fig. 4: Correlation between pseudo label inconsistency and noise. Pseudo labels are the average predictions from the teacher network across augmentations. Label noise is the SSI difference between ground truth and pseudo labels, while label inconsistency measures the SSI discrepancy between teacher outputs. The binned analysis shows that noise increases significantly in high inconsistency regions (80th percentile threshold = 1.0), indicating that higher inconsistency generally suggests larger pseudo label errors.

where  $t(\mathbf{d})$  is the median of  $\mathbf{d}$ , and  $s(\mathbf{d})$  is defined as:

$$s(\mathbf{d}) = \sum_{i=1}^{HW} |\mathbf{d}_i - t(\mathbf{d}_i)|. \quad (4)$$

In this way, we decouple the effects of scale and translation differences between datasets, enhancing the model’s focus on intrinsic predictive accuracy.

Several endoscopic datasets with depth annotations [19]–[24] are employed. Accurately annotating depth labels in endoscopic data presents a significant challenge compared to general open scenes because high-precision sensors are impractical to set up during clinical procedures. Consequently, existing datasets generate annotations using stereo cameras [20]–[22], registration to CT scans [19], [24], or synthetic data [23], [24]. To expand the training data, we have curated an additional dataset for bronchoscopy. Depth annotations are sourced using registration-based methods, airway meshes from patient CT scans are reconstructed, and video frames are manually registered to these in a virtual endoscopic view. Depth labels are generated by rendering depth maps in the airway model with the registered endoscopic poses. As a result, our teacher model leverages these extensive datasets, further enhancing training data diversity by generating pseudo-labels for unlabeled datasets to guide the student model training.

### B. Robust Student Model Training

To extend training data diversity for student model, besides labeled data from sources [19]–[24], we have incorporated unlabeled endoscopic data from datasets intended for other tasks [25]–[29], [42]. Each dataset introduces unique challenges due to variations in annotation accuracy—depth labels from stereo cameras can be sparse and imprecise due to calibration errors and environmental factors, while labels from registration methods may suffer from errors in registration and CT reconstruction inaccuracies. Leveraging this mix of unlabeled data enhances the breadth of our training data, yet introduces the risk of noisy pseudo-labels from the teacher model, which can mislead the student model’s training. This is particularly problematic in medical imaging, where fewer labeled data are available to train the teacher model, leading to its unstable performance on out-of-distribution unlabeled data. Such noise in training could result in degraded generalization performance during practical application. To address this, we propose to mitigate the impact of these inaccuracies by estimating the confidence of each labeled pixel. We then adjust the learning weight for each pixel based on its estimated confidence. This approach focuses gradient updates on regions with higher confidence, while reducing the influence of gradients from noisier regions.

**Learning Bias towards Clean Labeled Data.** Previous studies on learning from noisy labels in classification problems

have demonstrated that deep neural networks tend to first fit clean labels before potentially memorizing mislabeled ones [16]–[18]. This is because clean labels provide consistent and accurate gradient updates, leading to faster and more effective learning. The learning phenomenon has motivated a deeper examination of the teacher model’s training dynamics. Unlike classification tasks, SDE convergence can vary at a pixel level, depending on the precision of the annotations. We experiment with introducing annotation inaccuracies to the synthetic dataset SimColon [23] by misaligning image frames with depth labels, as depicted in Fig. 3. The teacher model rapidly converges for pixels with accurate labels, while those with noisy labels continue to exhibit elevated loss levels. This differential convergence pattern allows us to evaluate the confidence in each labeled pixel by examining their learning statuses as determined by the teacher model. Specifically, if the teacher model demonstrates early convergence at a pixel label, it suggests that the label is likely accurate. On the other hand, persistent non-convergence may signal potential inaccuracies. Based on these insights, we propose estimating the confidence of depth labels at each pixel using the formula:

$$p(\mathbf{d}_i | \mathbf{x}_i) \sim \rho(g(\mathbf{x}_i), \mathbf{d}_i), \quad (5)$$

where the confidence of depth labels are determined by the SSI discrepancy between manual labels and pretrained teacher model prediction based on Eq. 2.

To leverage this insight, we convert the label confidence into a weight map that prioritizes gradient updates from regions with higher confidence during training. This approach minimizes the influence of potentially less accurate regions on the network’s learning process. Accordingly, we define the weighted scale-and-shift invariant loss (WSSI) for labeled data formulated as:

$$L_{\text{wssi}}^{\text{labeled}} = \frac{1}{U} \sum_{i=1}^{HW} \mathbf{w}_i \cdot \rho(f(\mathbf{x}_i), \mathbf{d}_i), \quad (6)$$

where  $U = \sum_{i=1}^{HW} \mathbf{w}_i$  and the weight matrix  $\mathbf{w}$  is defined as:

$$\mathbf{w} = \exp\left(-\frac{\rho(g(\mathbf{x}), \mathbf{d})^2}{\tau_1}\right), \quad (7)$$

with the temperature parameter  $\tau_1$  empirically set to 0.5, based on preliminary experiments. This weight matrix applies an exponential decay based on the squared discrepancy between the manual labels and the teacher model’s predictions, ensuring a rapid reduction in the influence of label outliers on the overall training loss, while allowing contributions from labels that are more likely to be accurate.

**Learning Bias towards Clean Pseudo-labels.** Previous research in self-supervised learning for classification has shown that a model’s output for a sample is likely to be an accurate pseudo-label if it remains consistent across different augmentations of that sample [16]. We extend this analysis to monocular depth estimation by comparing the zero-shot

prediction errors of the teacher model and the inconsistencies in predictions across different data augmentations. As demonstrated in Fig 4, the pseudo-label error map closely aligns with the inconsistency map of the teacher model. Based on the observed output patterns, we hypothesize that the confidence of a pseudo-label can be estimated by the consistency of the teacher model’s outputs on different augmentations of the input sample. Formally, given an input  $x$  and a teacher model  $g$ , the confidence of a pseudo-label pixel can be expressed as:

$$p(g(\mathbf{x}_i) | \mathbf{x}_i) \sim \sigma\left(\{g(\hat{\mathbf{x}}_i^{(k)})\}_{k=1}^K\right), \quad (8)$$

where  $\sigma(\cdot)$  measures the consistency of estimates across augmented inputs  $\hat{\mathbf{x}}_i^{(k)}$ . For training efficiency, we simplify the confidence measurement by setting the number of augmentations  $K = 2$ , using random flipping and rotation. Consequently, we define the weighted scale-and-shift invariant loss (WSSI) for unlabeled data as:

$$L_{\text{wssi}}^{\text{unlabeled}} = \frac{1}{V} \sum_{i=1}^{HW} \mathbf{v}_i \cdot \rho(f(\mathbf{x}_i) - \bar{g}(\mathbf{x}_i)), \quad (9)$$

where  $V = \sum_{i=1}^{HW} \mathbf{v}_i$ . The pseudo label  $\bar{g}(\mathbf{x})$  is computed as  $\bar{g}(\mathbf{x}) = \frac{g(\mathbf{x}) + g(\hat{\mathbf{x}})}{2}$ , with  $\hat{\mathbf{x}}_i$  representing augmented version of  $\mathbf{x}_i$ . The weight matrix  $\mathbf{v}$  is defined as:

$$\mathbf{v} = \exp\left(-\frac{\rho(g(\mathbf{x}), g(\hat{\mathbf{x}}))^2}{\tau_2}\right), \quad (10)$$

with the temperature parameter  $\tau_2$  empirically set to 0.1 based on preliminary experiments. The weight for unlabeled data emphasizes reliable pseudo labels where the teacher model demonstrates higher consistency across different augmentations, and de-emphasizes contribution from uncertain pseudo labels to avoid disrupting student model training.

Compared to the trimmed scale-and-shift invariant loss (TSSI) [7], which relies on the instantaneous outputs of the student network to detect label outliers, our WSSI leverages a pretrained teacher model that has undergone additional training epochs, yielding more reliable error detection. Furthermore, instead of discarding a fixed percentage of data points, our method uses a soft weighting matrix that dynamically adjusts the influence of each data point, thus preserving the original data distribution.

### C. Removing the Ambiguous Shift Factor

To ensure a fair comparison with the latest research in medical image depth estimation, we fine-tune our foundation model  $f$  to create a refined model  $\hat{f}$  for zero-shot relative depth estimation (RDE), where only an unknown scale factor remains. Note that our main contribution remains the foundation model  $f$ . To address the shift ambiguity, we introduce a simple but effective third step: fine-tuning the student model  $f$  with a frozen encoder on the SCARED dataset using scale-invariant loss supervision. The SCARED dataset was chosen for its high annotation accuracy and sufficient training frames

TABLE II: Zero-shot RDE on Hamlyn Dataset.

Method	AbsRel $\downarrow$	SqRel $\downarrow$	RMSE $\downarrow$	RMSElog $\downarrow$	$\delta 1 \uparrow$
EDM* [34]	0.185	5.424	16.100	0.255	0.732
AF-SfMLearner* $\ddagger$ [35]	0.168	4.44	13.87	0.204	0.77
Surgical-DINO* [11]	0.146	3.216	11.974	0.178	0.801
EndoDAC* [12]	0.138	2.796	11.491	0.171	0.813
Depth-Anything* [9]	0.174	3.829	13.226	0.210	0.750
Depth-Anything2* [10]	0.229	5.949	16.718	0.269	0.649
Ours*	0.135	2.467	10.277	0.167	0.826
Ours $\triangle$	<b>0.097</b>	<b>1.286</b>	<b>7.687</b>	<b>0.123</b>	<b>0.875</b>

Best and second best performances are highlighted. \* denotes recovering scale before evaluation.  $\triangle$  denotes recovering scale and shift before evaluation.  $\ddagger$  denotes in-domain evaluation.

TABLE III: Zero-shot RDE on SERV-CT.

Method	AbsRel $\downarrow$	SqRel $\downarrow$	RMSE $\downarrow$	RMSElog $\downarrow$	$\delta 1 \uparrow$
SfMLearner* [44]	0.151	3.917	17.451	0.191	0.779
Fang et al.* [45]	0.149	3.099	15.564	0.188	0.787
DeFeat-Net* [46]	0.114	1.946	12.588	0.153	0.873
SC-SfMLearner* [47]	0.117	2.015	12.415	0.148	0.852
Monodepth2* [48]	0.123	2.205	12.927	0.152	0.856
Endo-SfM* [24]	0.116	2.014	12.493	0.143	0.864
AF-SfMLearner* [35]	0.102	1.632	11.092	0.131	0.898
Depth-Anything* [9]	0.080	0.906	7.212	0.098	0.928
Depth-Anything2* [10]	0.130	2.125	10.578	0.160	0.818
Ours*	0.060	0.445	5.511	0.075	0.988
Ours $\triangle$	<b>0.034</b>	<b>0.158</b>	<b>3.316</b>	<b>0.044</b>	<b>1.000</b>

Best and second best are highlighted. \* denotes recovering scale before evaluation.  $\triangle$  denotes recovering scale and shift before evaluation.

for fine-tuning. Formally, the pretrained student model  $f$  is fine-tuned on a single dataset using scale-invariant loss [43]:

$$L_{\text{si}} = \sqrt{\frac{1}{HW} \sum_{i=1}^{HW} (h_i)^2 - \frac{\lambda}{(HW)^2} \left( \sum_{i=1}^{HW} h_i \right)^2}, \quad (11)$$

where  $h_i^k = \log \hat{f}(\mathbf{x}_i)^k - \log y_i^k$  is the value of the log-depth difference map at position  $i$  and scale  $k$ .

During experiments, we included our scale-invariant fine-tuned version of model  $\hat{f}$  using the same median scaling preprocessing as existing methods to ensure a fair comparison.

#### IV. EXPERIMENTS

We conducted extensive experiments to evaluate the zero-shot relative depth estimation (RDE), fine-tuned to metric depth estimation (MDE), and zero-shot MDE on unseen datasets. We also analyzed the WSSI loss in ablation studies. Furthermore, we explored utilizing our depth estimation foundation model for other related tasks on endoscopic images.

##### A. Implementation Details

We adopt the DINOv2 [49] encoder and DPT [8] decoder for both the teacher and student models. We first train the teacher model on all labeled training sets until convergence. We then train the student model with a batch size of 32 until convergence under the teacher model's guidance. Following the approach in [9], we challenge the student model with

TABLE IV: Fine-tuned to MDE on Hamlyn Dataset.

Method	AbsRel $\downarrow$	SqRel $\downarrow$	RMSE $\downarrow$	RMSElog $\downarrow$	$\delta 1 \uparrow$
EDM-S [34]	0.235	7.045	17.500	0.253	0.671
EDM-MS [34]	0.327	10.693	25.009	0.440	0.337
Depth Anything [9]	0.135	2.264	10.046	0.167	0.810
Ours	<b>0.127</b>	<b>1.993</b>	<b>9.169</b>	<b>0.144</b>	<b>0.865</b>

EDM-S and EDM-MS correspond to Endo-Depth-and-Motion Stereo and Mono+Stereo respectively.

TABLE V: Fine-tuned to MDE on patient bronchoscopy dataset.

Method	AbsRel $\downarrow$	SqRel $\downarrow$	RMSE $\downarrow$	RMSElog $\downarrow$	$\delta 1 \uparrow$
Cycle-GAN [50]	1.153	18.594	13.26	0.736	0.185
DD-VNB [37]	0.656	5.443	7.631	0.554	0.320
Depth Anything [9]	0.404	1.270	2.761	0.364	0.482
Ours	<b>0.345</b>	<b>0.987</b>	<b>2.568</b>	<b>0.337</b>	<b>0.519</b>

strong perturbations including color jittering and Gaussian blurring. Additionally, a semantic perception technique aligning backbone features with DINOv2 [49] is adopted. Labeled data and unlabeled data are mixed in a 1:3 ratio for each input batch. For both teacher and student network training, we initialize the encoder with pretrained weights [9] for faster convergence and randomly initialize the decoder weights. We use a learning rate of  $5 \times 10^{-6}$  and a learning rate factor of 0.1:1 for the encoder and decoder. The networks are trained with the Adam optimizer with a linear decay learning rate.

##### B. Evaluation Metrics

We assess our approach using five widely recognized metrics in depth estimation: AbsRel (absolute relative error), SqRel (square relative error), RMSE (root mean square error), RMSElog (root mean square logarithmic error), and  $\delta 1$ , following established works [7], [9], [12], [34].

To align with existing research, we perform different preprocessing of depth estimation results for different experiments. We evaluate the foundation model  $f$  with per-frame scale  $s$  and shift  $t$  alignment with ground truth following [7]–[9] by solving:

$$(s, t) \leftarrow \arg \min_{s, t} \sum_{i=1}^H W(s \mathbf{d}_i + t - \mathbf{d}_i^*)^2. \quad (12)$$

For RDE comparison with existing medical imaging research, we perform median scaling [44] for the fine-tuned version model  $\hat{f}$  expressed by:

$$\tilde{\mathbf{d}} = \mathbf{d}^* \times \frac{\text{median}(\mathbf{d})}{\text{median}(\mathbf{d}^*)}. \quad (13)$$

For MDE estimation, we do not align depth prediction by any means. We note the preprocessing method used in the result tables.

##### C. Zero-shot Relative Depth Estimation

Compared with existing research on SDE in medical imaging, one important advantage of leveraging a foundation

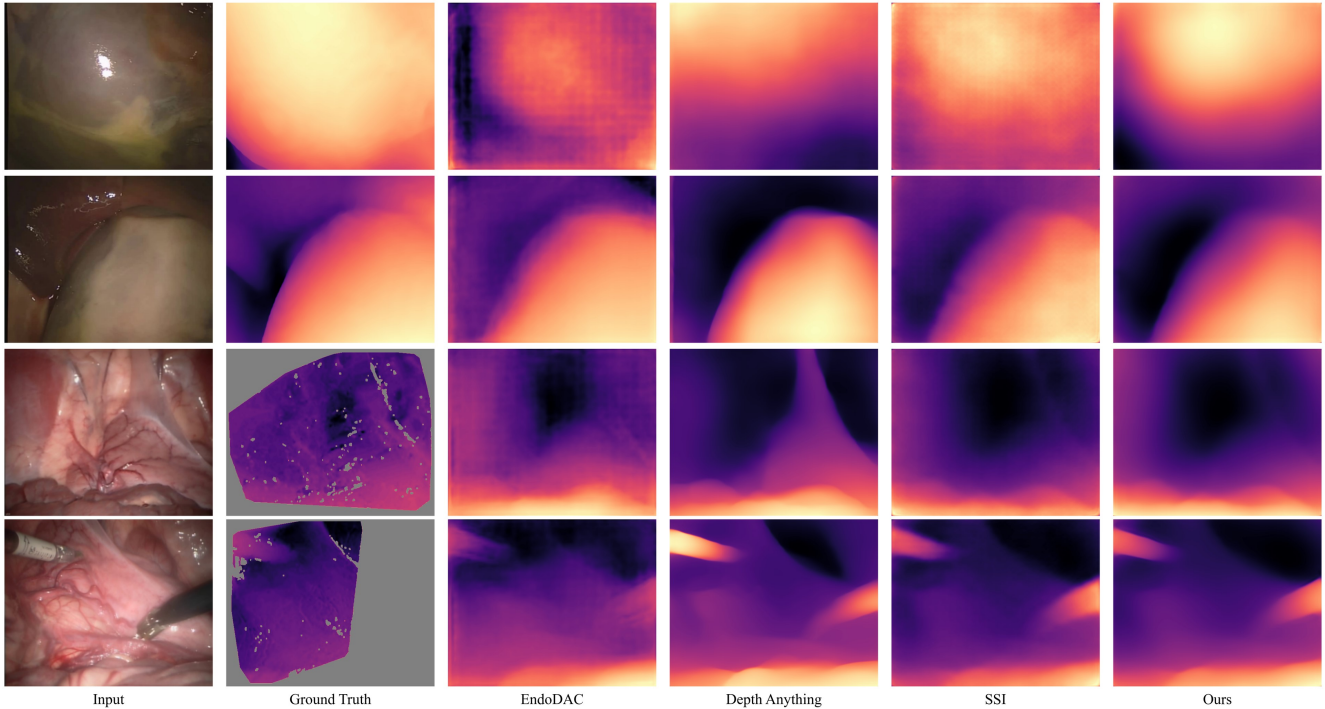


Fig. 5: Zero-shot performance of EndoOmni on SERV-CT (top two rows) and the Hamlyn Dataset (bottom two rows), compared with EndoDAC [12], the leading SOTA method for endoscopy, and Depth Anything [9], the top-performing SOTA foundation model. Quantitative results are also provided for the model without our robust training loss, denoted as SSI. EndoOmni demonstrates the most accurate geometric structure and the sharpest edges among all methods.

TABLE VI: Zero-shot MDE on phantom bronchoscopy dataset.

Method	AbsRel $\downarrow$	SqRel $\downarrow$	RMSE $\downarrow$	RMSElog $\downarrow$	$\delta_1\uparrow$
Cycle-GAN $^\ddagger$ [50]	0.433	3.460	7.091	0.407	0.355
DD-VNB $^\ddagger$ [37]	0.715	11.997	9.916	0.528	0.367
Depth-Anything [9]	0.508	4.280	9.430	0.576	0.329
<b>Ours</b>	<b>0.364</b>	<b>1.914</b>	<b>5.607</b>	<b>0.411</b>	<b>0.382</b>

$\ddagger$  denotes in-domain evaluation.

model trained on abundant mixed data is accurate depth estimation on unseen datasets during training. Therefore, we validate zero-shot RDE performance on two endoscopic datasets: Hamlyn and SERV-CT [20]. We follow existing works on MDE in medical imaging, fine-tuning the model on the SCARED dataset [22] at the third stage of training of our foundation model and use the same split scheme as existing works [11], [12], [34]. As shown in Table II and Table III, our model surpasses existing methods by a large margin. Notably, the best performing existing state-of-the-art (SOTA) method on the Hamlyn Dataset, EndoDAC [12], is a fine-tuned model of Depth Anything [9], which is trained on approximately 100 times the amount of data as our model. Compared with EndoDAC, we improve on all evaluated metrics, especially  $\text{RMSE}\downarrow$  (from 11.491 to 10.277) and  $\delta_1\uparrow$  (from 0.813 to 0.826), which suggests our model learns a tailored feature understanding for medical data through our large curated endoscopy datasets and advanced robust training schedule.

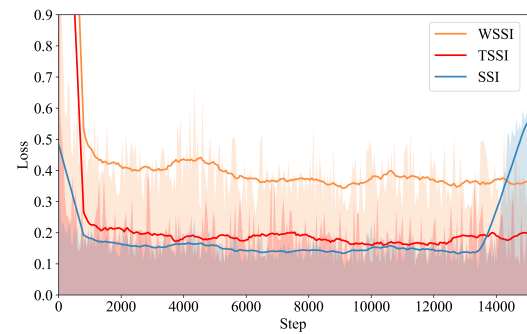


Fig. 6: Stability of training across different loss functions.

Quantitative results are shown in Fig. 5. Our EndoOmni provides the highest-quality outputs with well-defined edges.

#### D. Fine-tuned Metric Depth Estimation

Estimating depth with an absolute scale is critical for downstream tasks such as localization and mapping. However, only a limited amount of existing work in medical imaging focuses on predicting metric depth from monocular endoscopic images, likely due to the relatively small size of each individual dataset. Thus, we aim to provide a powerful foundation model as a promising initialization for fine-tuning MDE using a limited amount of data. Specifically, we initialize the encoder weight with our pretrained student model  $f$  and randomly initialize the decoder. The network is

TABLE VII: Ablation studies on baselines and losses.

Loss	SERV-CT					Hamlyn				
	AbsRel $\downarrow$	SqRel $\downarrow$	RMSE $\downarrow$	RMSElog $\downarrow$	$\delta 1\uparrow$	AbsRel $\downarrow$	SqRel $\downarrow$	RMSE $\downarrow$	RMSE log $\downarrow$	$\delta 1\uparrow$
Depth Anything [9]	0.041	0.25	3.986	0.053	0.996	0.100	1.330	7.858	0.126	0.869
Depth Anything v2 [10]	0.040	0.251	3.797	0.053	0.994	0.099	1.301	7.815	0.125	0.872
SSI [7]	0.038	0.174	3.420	0.047	0.999	0.098	1.304	7.756	0.125	0.874
TSSI [7]	0.037	0.169	3.399	0.047	1.000	0.100	1.331	7.850	0.126	0.870
Ours: WSSI-labeled	0.037	0.174	3.418	0.046	1.000	0.098	1.294	7.725	0.124	0.873
Ours: WSSI	<b>0.034</b>	<b>0.158</b>	<b>3.316</b>	<b>0.044</b>	<b>1.000</b>	<b>0.097</b>	<b>1.286</b>	<b>7.687</b>	<b>0.123</b>	<b>0.875</b>

Best and second best performances are highlighted. Recovered scale and shift for all results.

TABLE VIII: Fine-tuned to segmentation on Kvasir dataset.

Methods	Dice $\uparrow$	mIoU $\uparrow$	Recall $\uparrow$	Precision $\uparrow$	F2 $\uparrow$
TransNetR [51]	0.871	0.802	0.884	0.907	0.874
PraNet [52]	0.898	0.849	0.906	0.913	0.898
UACANet-S [53]	0.905	0.852	-	-	-
TGA-Net [54]	0.898	0.833	<b>0.913</b>	0.912	0.903
DINOv2 [49]	0.883	0.814	0.864	<b>0.941</b>	0.883
Ours	<b>0.909</b>	<b>0.857</b>	0.912	0.939	<b>0.909</b>

fine-tuned on a single dataset following the training strategy by [57].

**In-Domain Metric Depth Estimation.** We first evaluate in-domain MDE performance, where our model is fine-tuned and evaluated on the same datasets. We utilize the Hamlyn dataset and our bronchoscopy dataset for this experiment. For Hamlyn, we follow the split in [34], using sequences 1, 4, 19, and 20 for testing, and the rest for training. For the bronchoscopy dataset, we train and test our model on data recorded during regular inspection procedures for patients. Results are shown in Table IV and Table V. Our fine-tuned model surpasses existing methods on all evaluated metrics by a significant margin. By achieving state-of-the-art performance with fine-tuning for only a few epochs, our foundation model shows a generalized feature understanding ability that transfers to MDE on unseen datasets during training.

**Zero-Shot Metric Depth Estimation.** We further evaluate the zero-shot MDE performance of our model on phantom bronchoscopy data. We choose the model fine-tuned on our patient bronchoscopy data for their similar depth range, making it possible for zero-shot generalization. The evaluation test set of phantom data aligns with data used in [37]. As shown in Table VI, our model achieves better zero-shot MDE performance even when compared to methods that are tested on in-domain data. Furthermore, we compare using Depth Anything [9] pretrained weights to initialize the MDE model encoder and perform zero-shot MDE on phantom bronchoscopy data in Table VI. By training with our robust loss on abundant mixed endoscopic data, our model learns better endoscopy image representations and achieves better zero-shot MDE performance on all evaluated metrics.

### E. Ablation Studies

**Robust Training Loss.** We validate the effectiveness of our proposed robust training loss by analyzing the zero-shot RDE performance following the first two stages of training.

Since the second stage employs a scale-and-shift invariant loss, we evaluate RDE by aligning the per-frame scale and shift with ground truth. We compare the performance of four different training losses: (1) **SSI**, the standard scale-and-shift invariant loss initially proposed by MiDaS [7]; (2) **TSSI**, a loss proposed by [7], where outliers are identified and removed by trimming the largest loss residuals per instance; (3) **Ours: WSSI-labeled**, which incorporates the teacher model to assess ground truth confidence, enhancing learning bias for labeled data; and (4) **Ours: WSSI**, which is our complete weighted scale and shift invariant loss that extends confidence analysis to both labeled and unlabeled data. We evaluate these losses on the SERV-CT and Hamlyn datasets. As shown in Table VII, our WSSI consistently outperforms other methods across all metrics. Interestingly, we observe that trimming loss outliers, while intended to detect label noise, does not perform as expected on medical images. This supports our hypothesis that the trimming process may also discard hard-to-learn regions of each instance.

Additionally, we examine the training dynamics of the different losses, as shown in Fig. 6. Both WSSI and TSSI contribute to training stability, while the standard SSI loss leads to training collapse due to label noise interference. This results in premature underfitting, with the best-performing model on the validation set producing depth maps with blurred edges, as shown in Fig. 5. The performance degradation is particularly evident on the SERV-CT dataset, where accurate dense depth labels highlight the deficiencies of the vanilla SSI loss compared to the Hamlyn dataset.

**Comparison with Depth Anything.** Since EndoOmni initializes encoder weights from the general foundation model Depth Anything, we compare our zero-shot RDE performance to demonstrate the improvements on endoscopy data. We also include a comparison with the latest Depth Anything v2 for reference. As shown in Table VII, our EndoOmni outperforms all baselines across the evaluated metrics, particularly on the SERV-CT dataset, which offers more accurate dense depth labels, highlighting our model’s superior performance.

### F. Fine-tuned to Polyp Segmentation

Although originally trained for the SDE task, EndoOmni is expected to transfer effectively to other downstream tasks in endoscopy. To validate this capability, we applied EndoOmni to the task of polyp segmentation. We followed the data split of the established benchmark [52] and conducted ex-

TABLE IX: Branch-level endoscope localization accuracy by fine-tuning to airway lumen detection.

Methods	Case1*	Case2	Case3	Case4*	Case5	Case6	Case7*	Case8	Case9*	Case10	Case11	Mean Acc
AirwayNet [55]	64.33%	40.31%	26.92%	28.95%	46.36%	63.16%	30.89%	23.59%	38.11%	47.60%	15.29%	36.01%
BronchoTrack [56]	65.61%	24.26%	<b>91.15%</b>	44.87%	59.55%	60.77%	79.15%	10.77%	75.90%	74.50%	<b>40.00%</b>	51.68%
DINOv2 [49]	66.24%	70.96%	74.62%	66.58%	81.36%	88.04%	73.75%	82.05%	<b>86.97%</b>	76.20%	30.98%	69.65%
Ours	<b>75.16%</b>	<b>72.95%</b>	79.23%	<b>72.11%</b>	<b>90.00%</b>	<b>98.09%</b>	<b>85.33%</b>	<b>87.18%</b>	86.32%	<b>82.66%</b>	35.88%	<b>75.04%</b>

\* indicates the training cases for BronchoTrack. AirwayNet is trained using case-wise synthetic endoscopic frames. **Best** and second best are highlighted.

periments on the Kvasir-SEG dataset [58]. For this task, we modified EndoOmni by removing the final ReLU activation and adding batch normalization and dropout layers, without introducing any task-specific modules for segmentation. The results, shown in Table VIII, demonstrate that EndoOmni achieves superior performance compared to existing methods in medical imaging segmentation, highlighting its strong semantic representation capabilities. Additionally, compared with initialization with DINOv2 [49], we observed a significant improvement in Dice score from 0.883 to 0.909, underscoring EndoOmni’s potential as a versatile foundation model for multi-task applications in endoscopy.

#### G. Fine-tuned to Bronchoscopy Localization

To further evaluate EndoOmni’s transferability to other endoscopic tasks, we fine-tuned it to airway lumen detection. This problem, initially introduced by [55] and later used for branch-level endoscope localization in the airway [56]. We hypothesize that the geometric structure semantics learned during SDE training enable EndoOmni to transfer learning to anatomical understanding effectively. We initialized the pretrained EndoOmni encoder and employed a 3-layer MLP to detect airway branches in each frame. The final endoscope localization accuracy was evaluated using the same test set from [56]. As shown in Table IX, the fine-tuned EndoOmni outperformed existing specialized methods for branch-level endoscope localization. Additionally, we tested initializing the encoder with the powerful DINOv2 [49] pretrained weights, and EndoOmni still outperformed with a comfortable margin. This further indicates that EndoOmni could serve as a robust foundation for other downstream tasks in endoscopy.

## V. CONCLUSION

In this paper, we introduce EndoOmni, a depth estimation foundation model designed for endoscopy images. Leveraging large, diverse medical datasets and noise-robust loss functions, EndoOmni achieves state-of-the-art zero-shot performance, outperforming both existing methods specific to medical imaging and general-purpose foundation models. When fine-tuned on target datasets for metric depth estimation, the model serves as a powerful initializer, consistently delivering superior performance across both in-domain and out-of-domain scenarios. Moreover, EndoOmni demonstrates significant transferability to other tasks in the realm of endoscopy, surpassing DINOv2 by a considerable margin in polyp segmentation and bronchoscopy localization.

## REFERENCES

- [1] M. Ye, S. Giannarou, A. Meining, and G.-Z. Yang, “Online tracking and retargeting with applications to optical biopsy in gastrointestinal endoscopic examinations,” *Medical image analysis*, vol. 30, pp. 144–157, 2016.
- [2] M. Ye, E. Johns, A. Handa, L. Zhang, P. Pratt, and G.-Z. Yang, “Self-supervised siamese learning on stereo image pairs for depth estimation in robotic surgery,” in *The Hamlyn Symposium on Medical Robotics*, 2017, p. 27.
- [3] L. Maier-Hein, M. Wagner, T. Ross, *et al.*, “Heidelberg colorectal data set for surgical data science in the sensor operating room,” *Scientific data*, vol. 8, no. 1, p. 101, 2021.
- [4] J. Ju, C. W. Tseng, O. Bailo, G. Dikov, and M. Ghafoorian, “DG-Recon: Depth-guided neural 3d scene reconstruction,” in *ICCV*, 2023, pp. 18 184–18 194.
- [5] L. Kästner, V. C. Frasineanu, and J. Lambrecht, “A 3D-deep-learning-based augmented reality calibration method for robotic environments using depth sensor data,” in *ICRA*, 2020, pp. 1135–1141.
- [6] H. Huang, L. Li, H. Cheng, and S.-K. Yeung, “Photo-SLAM: Real-time simultaneous localization and photorealistic mapping for monocular stereo and rgb-d cameras,” in *CVPR*, 2024, pp. 21 584–21 593.
- [7] R. Ranftl, K. Lasinger, D. Hafner, K. Schindler, and V. Koltun, “Towards robust monocular depth estimation: Mixing datasets for zero-shot cross-dataset transfer,” *IEEE transactions on pattern analysis and machine intelligence*, vol. 44, no. 3, pp. 1623–1637, 2020.
- [8] R. Ranftl, A. Bochkovskiy, and V. Koltun, “Vision transformers for dense prediction,” in *ICCV*, 2021, pp. 12 179–12 188.
- [9] L. Yang, B. Kang, Z. Huang, X. Xu, J. Feng, and H. Zhao, “Depth anything: Unleashing the power of large-scale unlabeled data,” in *CVPR*, 2024, pp. 10 371–10 381.
- [10] L. Yang, B. Kang, Z. Huang, *et al.*, “Depth anything v2,” *arXiv preprint arXiv:2406.09414*, 2024.
- [11] B. Cui, M. Islam, L. Bai, and H. Ren, “Surgical-DINO: Adapter learning of foundation models for depth estimation in endoscopic surgery,” *International Journal of Computer Assisted Radiology and Surgery*, pp. 1–8, 2024.
- [12] B. Cui, M. Islam, L. Bai, A. Wang, and H. Ren, “EndoDAC: Efficient adapting foundation model for self-supervised depth estimation from any endoscopic camera,” *arXiv preprint arXiv:2405.08672*, 2024.
- [13] J. J. Han, A. Acar, C. Henry, and J. Y. Wu, “Depth anything in medical images: A comparative study,” *arXiv preprint arXiv:2401.16600*, 2024.
- [14] A. Gonzalez-Jimenez, S. Lionetti, P. Gottfrois, F. Gröger, M. Pouly, and A. A. Navarini, “Robust t-loss for medical image segmentation,” in *MICCAI*, 2023, pp. 714–724.
- [15] X. Zhon, Y. Sun, M. Deng, W. C. W. Chu, and Q. Dou, “Robust semi-supervised multimodal medical image segmentation via cross modality collaboration,” in *MICCAI*, 2024.

[16] T. Zhou, S. Wang, and J. Bilmes, “Robust curriculum learning: From clean label detection to noisy label self-correction,” in *ICLR*, 2020.

[17] S. Liu, J. Niles-Weed, N. Razavian, and C. Fernandez-Granda, “Early-learning regularization prevents memorization of noisy labels,” *NeurIPS*, vol. 33, pp. 20331–20342, 2020.

[18] Y. Li, H. Han, S. Shan, and X. Chen, “DISC: Learning from noisy labels via dynamic instance-specific selection and correction,” in *CVPR*, 2023, pp. 24070–24079.

[19] T. L. Bobrow, M. Golhar, R. Vijayan, V. S. Akshintala, J. R. Garcia, and N. J. Durr, “Colonoscopy 3D video dataset with paired depth from 2D-3D registration,” *Medical Image Analysis*, p. 102956, 2023.

[20] P. E. Edwards, D. Psychogios, S. Speidel, L. Maier-Hein, and D. Stoyanov, “SERV-CT: A disparity dataset from cone-beam ct for validation of endoscopic 3d reconstruction,” *Medical image analysis*, vol. 76, p. 102302, 2022.

[21] V. Penza, A. S. Ciullo, S. Moccia, L. S. Mattos, and E. De Momi, “EndoAbS dataset: Endoscopic abdominal stereo image dataset for benchmarking 3d stereo reconstruction algorithms,” *The International Journal of Medical Robotics and Computer Assisted Surgery*, vol. 14, no. 5, e1926, 2018.

[22] M. Allan, J. Mcleod, C. Wang, *et al.*, “Stereo correspondence and reconstruction of endoscopic data challenge,” *arXiv preprint arXiv:2101.01133*, 2021.

[23] A. Rau, P. E. Edwards, O. F. Ahmad, *et al.*, “Implicit domain adaptation with conditional generative adversarial networks for depth prediction in endoscopy,” *International journal of computer assisted radiology and surgery*, pp. 1–10.

[24] K. B. Ozyoruk, G. I. Gokceler, T. L. Bobrow, *et al.*, “EndoSLAM dataset and an unsupervised monocular visual odometry and depth estimation approach for endoscopic videos,” *Medical image analysis*, vol. 71, p. 102058, 2021.

[25] P. Azagra, C. Sostres, Á. Ferrández, *et al.*, “Endomapper dataset of complete calibrated endoscopy procedures,” *Scientific Data*, vol. 10, no. 1, p. 671, 2023.

[26] T. Roß, A. Reinke, P. M. Full, *et al.*, “Comparative validation of multi-instance instrument segmentation in endoscopy: Results of the robust-mis 2019 challenge,” *Medical image analysis*, vol. 70, p. 101920, 2021.

[27] S. Ali, F. Zhou, B. Braden, *et al.*, “An objective comparison of detection and segmentation algorithms for artefacts in clinical endoscopy,” *Scientific reports*, vol. 10, no. 1, p. 2748, 2020.

[28] A. Zia, K. Bhattacharyya, X. Liu, *et al.*, “Surgical visual domain adaptation: Results from the MICCAI 2020 SurgVis-Dom challenge,” *arXiv preprint arXiv:2102.13644*, 2021.

[29] J. Bernal, F. J. Sánchez, G. Fernández-Esparrach, D. Gil, C. Rodríguez, and F. Vilariño, “WM-DOVA maps for accurate polyp highlighting in colonoscopy: Validation vs. saliency maps from physicians,” *Computerized medical imaging and graphics*, vol. 43, pp. 99–111, 2015.

[30] S. F. Bhat, I. Alhashim, and P. Wonka, “Adabins: Depth estimation using adaptive bins,” in *CVPR*, 2021, pp. 4009–4018.

[31] S. F. Bhat, I. Alhashim, and P. Wonka, “Localbins: Improving depth estimation by learning local distributions,” in *ECCV*, 2022, pp. 480–496.

[32] L. Huynh, P. Nguyen-Ha, J. Matas, E. Rahtu, and J. Heikkilä, “Guiding monocular depth estimation using depth-attention volume,” in *ECCV*, 2020, pp. 581–597.

[33] L. Piccinelli, Y.-H. Yang, C. Sakaridis, *et al.*, “Unidepth: Universal monocular metric depth estimation,” in *CVPR*, 2024, pp. 10106–10116.

[34] D. Recasens, J. Lamarca, J. M. Fácil, J. Montiel, and J. Civera, “Endo-depth-and-motion: Reconstruction and tracking in endoscopic videos using depth networks and photo-metric constraints,” *IEEE Robotics and Automation Letters*, vol. 6, no. 4, pp. 7225–7232, 2021.

[35] S. Shao, Z. Pei, W. Chen, *et al.*, “Self-supervised monocular depth and ego-motion estimation in endoscopy: Appearance flow to the rescue,” *Medical image analysis*, vol. 77, p. 102338, 2022.

[36] X. Liu, A. Sinha, M. Ishii, *et al.*, “Dense depth estimation in monocular endoscopy with self-supervised learning methods,” *IEEE transactions on medical imaging*, vol. 39, no. 5, pp. 1438–1447, 2019.

[37] *DD-VNB: A Depth-based Dual-Loop Framework for Real-time Visually Navigated Bronchoscopy*, IROS, 2024.

[38] S. Mathew, S. Nadeem, S. Kumari, and A. Kaufman, “Augmenting colonoscopy using extended and directional cyclegan for lossy image translation,” in *CVPR*, 2020, pp. 4696–4705.

[39] M. Shen, Y. Gu, N. Liu, and G.-Z. Yang, “Context-aware depth and pose estimation for bronchoscopic navigation,” *IEEE Robotics and Automation Letters*, vol. 4, no. 2, pp. 732–739, 2019.

[40] R. Wei, B. Li, F. Zhong, *et al.*, “Absolute monocular depth estimation on robotic visual and kinematics data via self-supervised learning,” *IEEE Transactions on Automation Science and Engineering*, 2024.

[41] C. Zhang, S. Bengio, M. Hardt, B. Recht, and O. Vinyals, “Understanding deep learning (still) requires rethinking generalization,” *Communications of the ACM*, vol. 64, no. 3, pp. 107–115, 2021.

[42] C. I. Nwoye, T. Yu, C. Gonzalez, *et al.*, “Rendezvous: Attention mechanisms for the recognition of surgical action triplets in endoscopic videos,” *Medical Image Analysis*, vol. 78, p. 102433, 2022.

[43] D. Eigen, C. Puhrsch, and R. Fergus, “Depth map prediction from a single image using a multi-scale deep network,” in *NeurIPS*, vol. 27, Curran Associates, Inc., 2014.

[44] T. Zhou, M. Brown, N. Snavely, and D. G. Lowe, “Unsupervised learning of depth and ego-motion from video,” in *CVPR*, 2017, pp. 1851–1858.

[45] Z. Fang, X. Chen, Y. Chen, and L. V. Gool, “Towards good practice for CNN-based monocular depth estimation,” in *WACVW*, 2020, pp. 1091–1100.

[46] J. Spencer, R. Bowden, and S. Hadfield, “DeFeat-Net: General monocular depth via simultaneous unsupervised representation learning,” in *CVPR*, 2020, pp. 14402–14413.

[47] J. Bian, Z. Li, N. Wang, *et al.*, “Unsupervised scale-consistent depth and ego-motion learning from monocular video,” *NeurIPS*, vol. 32, 2019.

[48] C. Godard, O. Mac Aodha, M. Firman, and G. J. Brostow, “Digging into self-supervised monocular depth estimation,” in *ICCV*, 2019, pp. 3828–3838.

[49] M. Oquab, T. Darcret, T. Moutakanni, *et al.*, “DINOv2: Learning robust visual features without supervision,” *Transactions on Machine Learning Research Journal*, pp. 1–31, 2024.

[50] J.-Y. Zhu, T. Park, P. Isola, and A. A. Efros, “Unpaired image-to-image translation using cycle-consistent adversarial networks,” in *ICCV*, 2017, pp. 2223–2232.

[51] D. Jha, N. K. Tomar, V. Sharma, and U. Bagci, “TransNetR: Transformer-based residual network for polyp segmentation with multi-center out-of-distribution testing,” in *Medical Imaging with Deep Learning*, PMLR, 2024, pp. 1372–1384.

[52] D.-P. Fan, G.-P. Ji, T. Zhou, *et al.*, “Pranet: Parallel reverse attention network for polyp segmentation,” in *MICCAI*, 2020, pp. 263–273.

[53] T. Kim, H. Lee, and D. Kim, “UACANet: Uncertainty augmented context attention for polyp segmentation,” in *ACM MM*, 2021, pp. 2167–2175.

- [54] N. K. Tomar, D. Jha, U. Bagci, and S. Ali, “TGANet: Text-guided attention for improved polyp segmentation,” in *MICCAI*, 2022, pp. 151–160.
- [55] J. Sganga, D. Eng, C. Graetzel, and D. B. Camarillo, “Autonomous driving in the lung using deep learning for localization,” *arXiv preprint arXiv:1907.08136*, 2019.
- [56] Q. Tian, H. Liao, X. Huang, *et al.*, “BronchoTrack: Airway lumen tracking for branch-level bronchoscopic localization,” *arXiv preprint arXiv:2402.12763*, 2024.
- [57] S. F. Bhat, R. Birkl, D. Wofk, P. Wonka, and M. Müller, “Zoedepth: Zero-shot transfer by combining relative and metric depth,” *arXiv preprint arXiv:2302.12288*, 2023.
- [58] D. Jha, P. H. Smedsrød, M. A. Riegler, *et al.*, “Kvasir-SEG: A segmented polyp dataset,” in *MMM*, 2020, pp. 451–462.